nature geoscience

ARTICLES

https://doi.org/10.1038/s41561-021-00756-7

Dry metastable olivine and slab deformation in a wet subducting slab

Takayuki Ishii[1,2] ✉ and Eiji Ohtani[3]

A widely accepted explanation for deep-focus earthquakes is that they are caused by the delayed transformation kinetics of dry olivine, which would seem to require dry subducting slabs. However, many geochemical and geophysical observations and mineral physics data indicate that water is present within both hydrous and nominally anhydrous minerals, implying hydrated subducting slabs. The presence of metastable olivine in wet slabs is therefore paradoxical, and the hydration state of the slabs remains an open question. Here, we report results of water-partitioning experiments between olivine, wadsleyite and a major dense hydrous magnesium silicate in slabs, hydrous phase A, under water-undersaturated conditions. We show that olivine and wadsleyite coexisting with hydrous phase A are kinetically dry and contain less than 1 ppm and approximately 300 ppm water, respectively. Our results suggest that olivine and wadsleyite show dry transformation kinetics even in wet slabs. It is therefore possible that olivine transformation as a cause of deep-focus earthquakes and large slab deformation creating stagnant slabs could occur in the water-undersaturated wet slabs. These processes could be caused jointly by dehydration of hydrous minerals and the subsequent rapid phase transformation when the dehydration starts at lower temperatures than the phase transformation.

Water in mantle minerals plays very important roles in mantle dynamics; that is, water in nominally anhydrous minerals such as olivine enhances the diffusion of atoms, deformation of minerals due to hydrolytic weakening[1,2] and transformation kinetics[3]. Subducting slabs transport water into the deep mantle by nominally anhydrous and hydrous minerals. Therefore, the amount of water in nominally anhydrous minerals together with the stability of hydrous minerals is one of the most important factors to control the dynamics of slab subduction.

Olivine, which is the most abundant mineral in Earth's upper mantle, transforms to high-pressure polymorphs of wadsleyite and ringwoodite at depths of 410 km and 520 km, respectively, in the mantle transition zone. However, the transformations of olivine in the cold interiors of subducting slabs occur at deeper regions than its equilibrium phase boundary due to relatively low slab temperature and therefore sluggish kinetics of transformations[4,5]. Thus, metastable olivine can exist even at the bottom of the transition zone.

In some slabs, metastable olivine has been observed by seismological studies as low-velocity regions in the interior of slabs, for example, beneath the Sea of Japan and the Mariana Trough down to 580–630 km deep[6,7]. These regions have been called metastable olivine wedges. The phase transformation of olivine in the metastable olivine wedge might cause deep-focus earthquakes[8–10]. These observations have been interpreted to be a signature of dry slabs[11,12] because even small amounts of water (several hundred ppm) enhance the transformation kinetics of olivine[3,13,14], leading to the absence of a metastable olivine wedge. However, we expect that slabs generally contain water as hydrous minerals such as chlorite, serpentine and hydrous phase A[15–17]. The intermediate-depth earthquakes are triggered by dehydration of hydrous minerals, and the double seismic zone is observed in the slab exceeding 50 km inward from its surface, which indicates the region of dehydration. The aseismic zone with the thickness of ~40 km between the upper and lower seismic zones would be a cold hydrated core, which transports water into the deep upper mantle[16,18,19]. A water content in slabs in the deep upper mantle has been estimated to be at least 1,600–3,500 ppm on average on the basis of mineral physics data and seismological observations[16,18,19]. The variation of the estimation depends on the thermal structures of hot and cold slabs. Hydration mechanisms of slabs before subduction such as fractures in slabs produced by slab bending and water supply into slabs by upwelling plumes[20–24] also support the cold hydrated core of the slab. If this is the case, the existence of a metastable olivine wedge in the wet slabs is a paradox due to the fast transformation kinetics of wet olivine. It is thus crucial for understanding the dynamics of slab subduction to clarify whether the existence of metastable olivine wedges is a real signature of dry slabs.

To solve the paradox, the water solubilities of olivine and its high-pressure polymorphs coexisting with hydrous minerals are essential. Most of the previous studies on water solubility in these minerals have focused on the solubility limit at temperatures outside the metastable olivine wedges, which are above the stability fields of hydrous minerals (>1,000 °C)[25,26], under water-saturated conditions (the 'water storage capacity')[27–29]. Therefore, in this work we have conducted water-partitioning experiments between olivine or wadsleyite and coexisting hydrous phase A (whose compositions fall along the forsterite–brucite and forsterite–water joins) below 1,000 °C under water-undersaturated conditions.

We measured water contents of forsterite and wadsleyite coexisting with hydrous phase A under pressure and temperature conditions corresponding to cold regions of subducting slabs in the deep upper mantle (8–12 GPa and 700–900 °C)[26] (Extended Data Table 1). The water contents were measured with single crystals of forsterite and wadsleyite using Fourier transform infrared (FTIR) spectroscopy. To measure precise water contents in the crystals, we set a pre-synthesized 200–400 μm single crystal of forsterite or wadsleyite enclosed in a magnesium silicate powdered mixture containing

[1]Center for High Pressure Science and Technology Advanced Research, Beijing, China. [2]Bayerisches Geoinstitut, University of Bayreuth, Bayreuth, Germany. [3]Department of Earth Sciences, Graduate School of Science, Tohoku University, Aoba, Sendai, Japan. ✉e-mail: takayuki.ishii@hpstar.ac.cn

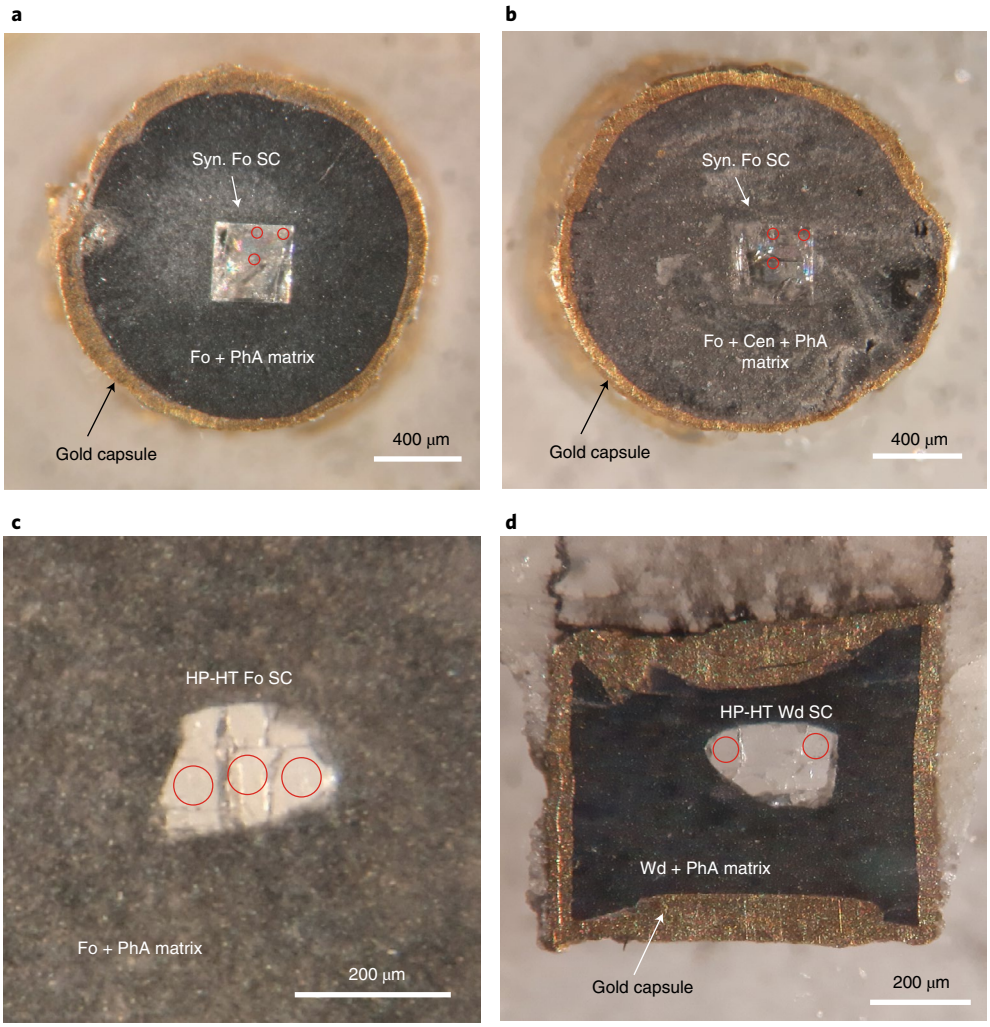

Fig. 1 | Representative photographs of cross sections of recovered samples. a, 10 GPa and 800 °C (H5150). **b**, 10 GPa and 800 °C (H5150). **c**, 10 GPa and 800 °C (S7423). **d**, 12 GPa and 900 °C (H5073). Syn. Fo SC, starting forsterite single crystal with <1 ppm water; HP-HT Fo SC, starting Fo SC with 29 ± 9 ppm water; HP-HT Wd SC, starting wadsleyite SC with 342 ± 103 ppm water. Powdered mixtures recovered are Fo or Wd + hydrous phase A (PhA) or Fo or Wd + PhA + clinoenstatite (Cen). Red circles are locations for the FTIR measurements.

brucite as a water source (Extended Data Fig. 1). We prepared two powdered mixtures with Mg/Si ratios of 2.25 and 2.00 (8Fo + 2Br and 8Fo + 2[2Br + Qz], respectively) (Methods). In all run products, we clearly observed single crystals of forsterite or wadsleyite surrounded by the polycrystalline mixture (Fig. 1). Recovered polycrystalline mixtures were identified to be forsterite or wadsleyite plus hydrous phase A in 8Fo + 2Br and forsterite or wadsleyite plus hydrous phase A with an additional nominally anhydrous mineral of clinoenstatite in 8Fo + 2[2Br + Qz] (Extended Data Table 1 and Extended Data Fig. 2).

Micro-FTIR spectra of the starting materials and recovered samples of forsterite and wadsleyite single crystals were measured at ambient conditions (Extended Data Tables 1 and 2 and Fig. 2). Before the experiments, we prepared two kinds of forsterite single crystals: one is synthetic forsterite with less than 1 ppm water produced at one atmosphere and high temperature and the other is forsterite with 29 ± 9 ppm water synthesized at high pressure and high temperature (Methods). We also prepared the starting crystal of wadsleyite with 342 ± 103 ppm water synthesized at high pressure and high temperature. Effects of crystal orientation on their FTIR spectra seem not to be notable because different crystal orientations of forsterite and wadsleyite provided similar FTIR spectra (Fig. 2, Extended Data Tables 1 and 2 and Supplementary Figs. 1–3). No difference in the water contents was observed in a run duration of 12–72 h at 700–800 °C even though we measured the water contents close to the hydrous silicate matrix with the distance of 20–50 μm using FTIR (Fig. 1). However, hydrogen diffusion in wadsleyite is by one to two orders of magnitude faster than that in forsterite[30], indicating that the run duration of 13–14 h is sufficient. Water contents of the recovered single crystals of forsterite and wadsleyite were determined to be less than 1 ppm and 187–370 ppm with 30% errors, respectively, which show that the water contents seem to be less than those of the starting materials within the uncertainty of the measurements. Results of reversal experiments using hydrous forsterite or wadsleyite show that hydrogen in forsterite or wadsleyite migrates into an aggregate of dry forsterite or wadsleyite + hydrous phase A ± clinoenstatite on the basis of the following reaction: $5Mg_2SiO_4$ (forsterite/wadsleyite) + $3H_2O \rightarrow Mg_7Si_2O_8(OH)_6$ (Phase A) + $3MgSiO_3$ (clinoenstatite)[25]. Formation of hydrous phase A is thus preferred rather than hydration of forsterite or wadsleyite at pressure–temperature conditions in which hydrous phase A is stable. These results indicate that forsterite and wadsleyite coexisting with hydrous phase A in water-undersaturated conditions are very dry in both excess-Mg and excess-Si systems. One may consider the

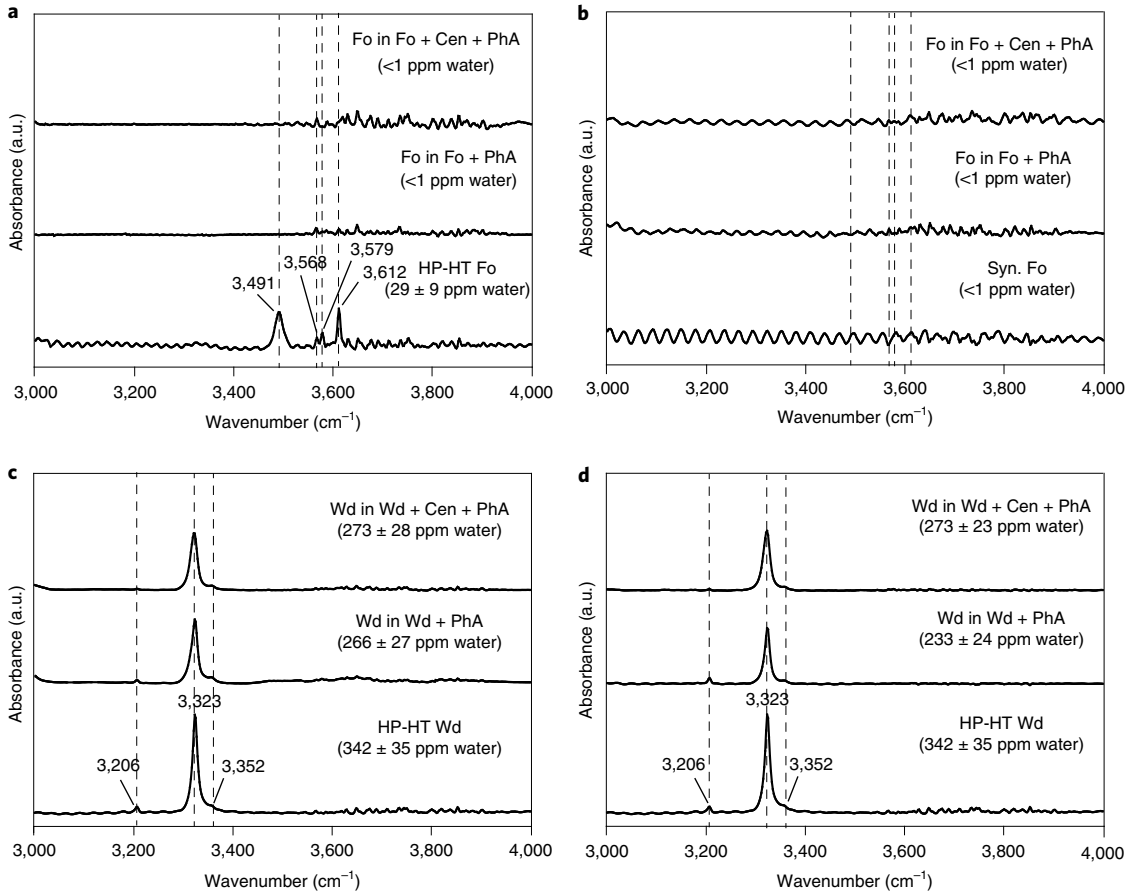

Fig. 2 | Representative unpolarized FTIR spectra of forsterite and wadsleyite single crystals coexisting with hydrous phase A. a, 10 GPa and 800 °C (S7423). **b**, 10 GPa and 800 °C (H5150). **c**, 12 GPa and 900 °C (H5073). **d**, 12 GPa and 800 °C (H5085). The bottom spectra are those of starting single crystals of forsterite or wadsleyite.

effect of Fe on hydrogen diffusion. Previous studies, however, demonstrated that the effect is negligible for olivine and wadsleyite[31–33], implying that our Fe-free results can be applied to natural processes. In the mantle, olivine and its polymorphs coexist with other anhydrous minerals such as pyroxene and garnet. Water might be partitioned into these minerals. However, these minerals will be also essentially dry when we consider water partitioning between dry olivine/its polymorphs and these minerals[34]. It would be important to investigate water contents in these minerals coexisting with olivine and hydrous minerals in the future for a better understanding of the water transport into the deep mantle by our experimental strategy.

Dry olivine and wadsleyite coexisting with hydrous phase A

Water contents in recovered forsterite and wadsleyite single crystals are plotted in Fig. 3a,b together with their previous reports under water-saturated conditions[29]. Olivine and wadsleyite contain very small amounts of water, less than 1 ppm and 300 ppm below 1,000 °C, respectively, under water-undersaturated conditions. However, we clearly see a drastic increase of water contents in both olivine and wadsleyite associated with dehydration of hydrous minerals around 1,000 °C due to a rapid increase in water fugacity of the system. This increase of the water contents implies that, once wet slabs are heated to dehydration temperatures of hydrous minerals around 1,000 °C, olivine and wadsleyite incorporate a large amount of water. The increase of the water contents in olivine and wadsleyite by water release from hydrous minerals would enhance the transformation kinetics of olivine and rheology of olivine and its polymorphs[2,3,13,14], resulting in a large deformation of the slabs as discussed in the following.

Dry transformation kinetics in wet descending slab

Our results of dry forsterite and wadsleyite coexisting with hydrous phase A can explain the paradoxical existence of the metastable olivine wedge in wet subducting slabs on the basis of their transformation kinetics. It has been reported that the kinetics of the olivine–wadsleyite transformation strongly depend on the water content in these minerals[13,35]. These experiments showed that metastable olivine containing 500 ppm water can survive up to the base of the mantle transition zone at low temperatures of around 600 °C, which have been considered to be within the internal slab temperature range (500–700 °C (ref. [26])). In addition, the ringwoodite growth rate from olivine with more than 75 ppm water is enhanced by hydrolytic weakening, suggesting the metastable olivine wedge should be produced by olivine with less than 75 ppm water[14]. Our study indicates that the metastable olivine wedge can exist under wet but water-undersaturated conditions; that is, the existence of the metastable olivine wedge is not the signature of dry descending slabs, but it would be the signature of water-undersaturated conditions coexisting with hydrous minerals.

It has been considered that deep-focus earthquakes are generated by the phase transformation of metastable olivine[4,8–10]. The results of the present study revealed that this mechanism

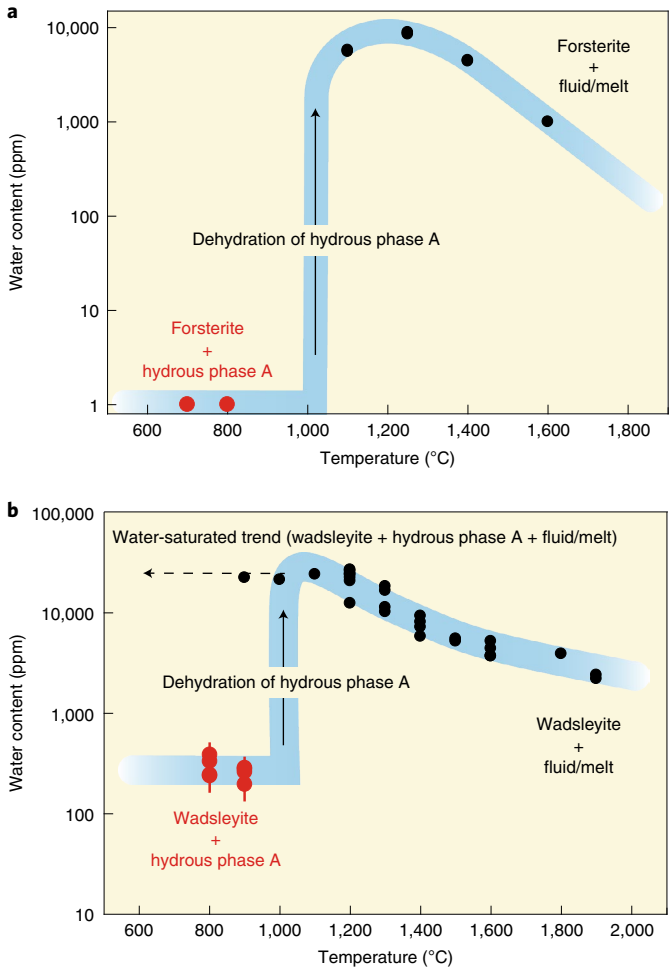

Fig. 3 | The water content in forsterite at 8–12 GPa and wadsleyite at 12–20 GPa with increasing temperature. a,**b**, Drastic increases of water content are observed in forsterite (**a**) and wadsleyite (**b**) due to dehydration of hydrous phase A. Red and black solid circles are data reported by this study and previous studies[28,29], respectively. Note that previous studies conducted experiments under water-saturated conditions, resulting in high water contents in wadsleyite under coexistence with hydrous phase A. The arrows indicate the increase of the water content in olivine and wadsleyite due to dehydration of hydrous phase A.

works even in water-undersaturated wet slabs. Deep-focus earthquakes may also be triggered by dehydration of hydrous minerals as proposed for intermediate-depth earthquakes[36]. On the basis of the kinetics of the olivine–wadsleyite transformation[3], a thermochemical study found a 'blocking temperature' of the olivine–wadsleyite transformation to be 725 °C and applied it to the metastable olivine wedge in the Marianas slab[37]. However, a numerical study analysed the kinetics of this phase transformation and demonstrated that the temperature for completion of 10–90% transformation is 700 °C for 200 ppm water[38]. Thus, the blocking temperature could be much higher for olivine with water content less than 1 ppm as demonstrated in this study and could rise to the dehydration temperature of hydrous phase A[13]. We also emphasize that the breakdown temperatures of hydrous phases have not been determined under water-undersaturated conditions, where the breakdown temperatures might be lower due to the low water fugacity. Therefore, the present results might support the argument that dehydration may continue to play an important seismogenic role for deep-focus earthquakes[39].

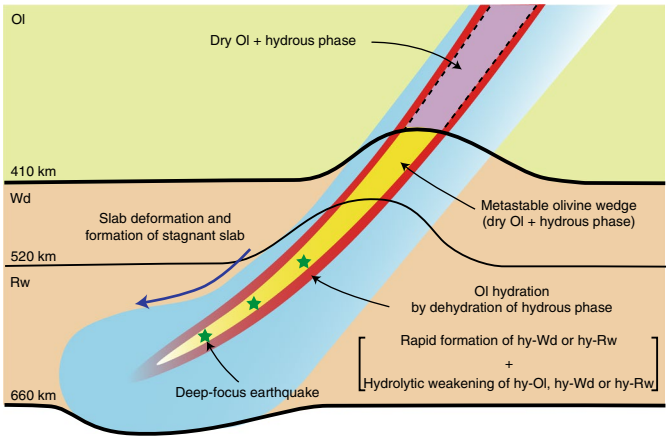

Fig. 4 | Slab deformation and formation of a stagnant slab in a wet descending slab and their possible linkage with dehydration of hydrous phases. The presence of hydrous phases (<1,000 °C) and dry metastable olivine (Ol) core (<700–1,000 °C) along the isotherms shaded as yellow. In the temperature region of the slab above 1,000 °C (red-shaded area), dehydration of hydrous phases and increase of the water fugacity create Ol and its high-pressure polymorphs of wadsleyite (Wd) and ringwoodite (Rw) with high water contents (hydrated (hy)-Ol, hy-Wd and hy-Rw, respectively), which possibly links with slab deformation, resulting in a stagnant slab.

Slab deformation in wet descending slab

The present results showed that olivine and wadsleyite coexisting with hydrous phase A are essentially dry, and water is stored in hydrous phase A. Therefore, the rheological property for the phase transformation under the dry condition[40] can be applied to the water-undersaturated slab. An exothermic phase transformation-induced grain-size reduction in the slabs could cause slab softening while the slabs are warming[41–43], with large deformation of the slabs contributing to the formation of stagnant slabs[44]. The drastic change in water contents of olivine and wadsleyite associated with the dehydration of hydrous phase A may provide notable effects on the rheology of slabs. The slab weakening might be linked to the rapid phase transformation kinetics[3,13] and hydrolytic weakening[45] of wet olivine induced by fluids from dehydration of hydrous phase A[46] when the blocking temperature of the olivine–wadsleyite transformation is comparable to or higher than the dehydration temperature of hydrous phase A as shown in the preceding. Processes in the water-undersaturated slab are shown in Fig. 4.

In mantle transition zone conditions, other hydrous minerals rather than hydrous phase A, such as hydrous phase E and superhydrous phase B, could be stable and coexist with wadsleyite or ringwoodite. However, it is likely that water will be strongly partitioned into other hydrous phases, according to our results. The reason for strong water partitioning into hydrous phase A would be closely related to a stable O–H geometry and stronger O–H bonding nature in their crystal structures, compared with those in forsterite and its polymorphs[47,48]. The stable O–H geometry and strong O–H bonding nature would be common in other hydrous minerals as demonstrated in hydrous phase E[49] and superhydrous phase B[50]. The water partitioning between nominally anhydrous minerals and other high-pressure hydrous phases stable in the mantle transition zone and the effect of iron on the water partitioning should be studied in the future to further strengthen our hypothesis.

Online content

Any methods, additional references, Nature Research reporting summaries, source data, extended data, supplementary information, acknowledgements, peer review information; details of

author contributions and competing interests; and statements of data and code availability are available at https://doi.org/10.1038/s41561-021-00756-7.

Received: 8 June 2020; Accepted: 20 April 2021;
Published online: 24 May 2021

References

1. Mei, S. & Kohlstedt, D. L. Influence of water on plastic deformation of olivine aggregates: 2. Dislocation creep regime. *J. Geophys. Res. Solid Earth* **105**, 21471–21481 (2000).
2. Karato, S. I. & Jung, H. Effects of pressure on high-temperature dislocation creep in olivine. *Philos. Mag. A* **83**, 401–414 (2003).
3. Kubo, T., Ohtani, E., Kato, T., Shinmei, T. & Fujino, K. Effects of water on the α–β transformation kinetics in San Carlos olivine. *Science* **281**, 85–87 (1998).
4. Sung, C. M. & Burns, R. G. Kinetics of the olivine→spinel transition: implications to deep-focus earthquake genesis. *Earth Planet. Sci. Lett.* **32**, 165–170 (1976).
5. Perrillat, J. P. et al. Kinetics of the olivine–ringwoodite transformation and seismic attenuation in the Earth's mantle transition zone. *Earth Planet. Sci. Lett.* **433**, 360–369 (2016).
6. Iidaka, T. & Suetsugu, D. Seismological evidence for metastable olivine inside a subducting slab. *Nature* **356**, 593–595 (1992).
7. Jiang, G., Zhao, D. & Zhang, G. Seismic evidence for a metastable olivine wedge in the subducting Pacific slab under Japan Sea. *Earth Planet. Sci. Lett.* **270**, 300–307 (2008).
8. Kirby, S. Mantle phase changes and deep-earthquake faulting in subducting lithosphere. *Science* **252**, 216–224 (1991).
9. Green, H. W. II & Houston, H. The mechanisms of deep earthquakes. *Annu. Rev. Earth Planet. Sci.* **23**, 169–213 (1995).
10. Schubnel, A. et al. Deep-focus earthquake analogs recorded at high pressure and temperature in the laboratory. *Science* **341**, 1377–1380 (2013).
11. Kawakatsu, H. & Yoshioka, S. Metastable olivine wedge and deep dry cold slab beneath southwest Japan. *Earth Planet. Sci. Lett.* **303**, 1–10 (2011).
12. Green, H. W. II, Chen, W. P. & Brudzinski, M. R. Seismic evidence of negligible water carried below 400-km depth in subducting lithosphere. *Nature* **467**, 828–831 (2010).
13. Hosoya, T., Kubo, T., Ohtani, E., Sano, A. & Funakoshi, K. I. Water controls the fields of metastable olivine in cold subducting slabs. *Geophys. Res. Lett.* **32**, L17305 (2005).
14. Du Frane, W. L., Sharp, T. G., Mosenfelder, J. L. & Leinenweber, K. Ringwoodite growth rates from olivine with ~75 ppmw H_2O: metastable olivine must be nearly anhydrous to exist in the mantle transition zone. *Phys. Earth Planet. Inter.* **219**, 1–10 (2013).
15. Peslier, A. H., Schönbächler, M., Busemann, H. & Karato, S. I. Water in the Earth's interior: distribution and origin. *Space Sci. Rev.* **212**, 743–810 (2017).
16. Hacker, B. R., Peacock, S. M., Abers, G. A. & Holloway, S. D. Subduction factory 2. Are intermediate-depth earthquakes in subducting slabs linked to metamorphic dehydration reactions? *J. Geophys. Res. Solid Earth* **108**, 2030 (2003).
17. Schmidt, M. W. & Poli, S. Experimentally based water budgets for dehydrating slabs and consequences for arc magma generation. *Earth Planet. Sci. Lett.* **163**, 361–379 (1998).
18. Yamasaki, T. & Seno, T. Double seismic zone and dehydration embrittlement of the subducting slab. *J. Geophys. Res.* **108**, 2212 (2003).
19. van Keken, P. E., Hacker, B. R., Syracuse, E. M. & Abers, G. A. Subduction factory: 4. Depth-dependent flux of H_2O from subducting slabs worldwide. *J. Geophys. Res.* **116**, 1401 (2011).
20. Peacock, S. M. Are the lower planes of double seismic zones caused by serpentine dehydration in subducting oceanic mantle? *Geology* **29**, 299–302 (2001).
21. Seno, T. & Yamanaka, Y. in *Subduction: Top to Bottom* (eds Bebout, G. E. et al.) 347–355 (AGU, 1996).
22. Hirano, N. et al. Volcanism in response to plate flexure. *Science* **313**, 1426–1428 (2006).
23. Cai, C., Wiens, D. A., Shen, W. & Eimer, M. Water input into the Mariana subduction zone estimated from ocean-bottom seismic data. *Nature* **563**, 389–392 (2018).
24. Ranero, C. R., Morgan, J. P., McIntosh, K. & Reichert, C. Bending-related faulting and mantle serpentinization at the Middle America trench. *Nature* **425**, 367–373 (2003).
25. Komabayashi, T., Omori, S. & Maruyama, S. Petrogenetic grid in the system $MgO–SiO_2–H_2O$ up to 30 GPa, 1600 °C: applications to hydrous peridotite subducting into the Earth's deep interior. *J. Geophys. Res.* **109**, B03206 (2004).
26. Kirby, S. H., Okal, E. A., Stein, S. & Rubie, D. C. Metastable mantle phase transformations and deep earthquake in subducting oceanic lithosphere. *Rev. Geophys.* **34**, 261–306 (1996).
27. Bolfan-Casanova, N. Water in the Earth's mantle. *Mineral. Mag.* **69**, 229–257 (2005).
28. Smyth, J. R., Frost, D. J., Nestola, F., Holl, C. M. & Bromiley, G. Olivine hydration in the deep upper mantle: effects of temperature and silica activity. *Geophys. Res. Lett.* **33**, L15301 (2006).
29. Litasov, K. D., Shatskiy, A., Ohtani, E. & Katsura, T. Systematic study of hydrogen incorporation into Fe-free wadsleyite. *Phys. Chem. Miner.* **38**, 75–84 (2011).
30. Hae, R., Ohtani, E., Kubo, T., Koyama, T. & Utada, H. Hydrogen diffusivity in wadsleyite and water distribution in the mantle transition zone. *Earth Planet. Sci. Lett.* **243**, 141–148 (2006).
31. Demouchy, S. & Mackwell, S. Water diffusion in synthetic iron-free forsterite. *Phys. Chem. Miner.* **30**, 486–494 (2003).
32. Demouchy, S. & Mackwell, S. Mechanisms of hydrogen incorporation and diffusion in iron-bearing olivine. *Phys. Chem. Miner.* **33**, 347–355 (2006).
33. Kudo, T., Ohtani, E., Hae, R. & Shimojuku, A. Diffusion of hydrogen in ringwoodite. *AIP Conf. Proc.* **833**, 148–149 (2006).
34. Keppler, H. & Bolfan-Casanova, N. Thermodynamics of water solubility and partitioning. *Rev. Mineral. Geochem.* **62**, 193–230 (2006).
35. Kubo, T., Ohtani, E. & Funakoshi, K. I. Nucleation and growth kinetics of the α–β transformation in Mg_2SiO_4 determined by in situ synchrotron powder X-ray diffraction. *Am. Mineral.* **89**, 285–293 (2004).
36. Ferrand, T. P. et al. Dehydration-driven stress transfer triggers intermediate-depth earthquakes. *Nat. Commun.* **8**, 15247 (2017).
37. Quinteros, J. & Sobolev, S. V. Constraining kinetics of metastable olivine in the Marianas slab from seismic observations and dynamic models. *Tectonophysics* **526**, 48–55 (2012).
38. Yoshioka, S., Torii, Y. & Riedel, M. R. Impact of phase change kinetics on the Mariana slab within the framework of 2-D mantle convection. *Phys. Earth Planet. Inter.* **240**, 70–81 (2015).
39. Zahradnik, J. et al. A recent deep earthquake doublet in light of long-term evolution of Nazca subduction. *Sci. Rep.* **7**, 45153 (2017).
40. Karato, S. I., Riedel, M. R. & Yuen, D. A. Rheological structure and deformation of subducted slabs in the mantle transition zone: implications for mantle circulation and deep earthquakes. *Phys. Earth Planet. Inter.* **127**, 83–108 (2001).
41. Mohiuddin, A., Karato, S. I. & Girard, J. Slab weakening during the olivine to ringwoodite transition in the mantle. *Nat. Geosci.* **13**, 170–174 (2020).
42. Čížková, H., van Hunen, J., van den Berg, A. P. & Vlaar, N. J. The influence of rheological weakening and yield stress on the interaction of slabs with the 670 km discontinuity. *Earth Planet. Sci. Lett.* **199**, 447–457 (2002).
43. Rosa, A. D. et al. Evolution of grain sizes and orientations during phase transitions in hydrous Mg_2SiO_4. *J. Geophys. Res.* **121**, 7161–7176 (2016).
44. Fukao, Y., Obayashi, M. & Nakakuki, T. & Deep Slab Project Group. Stagnant slab: a review. *Annu. Rev. Earth Planet. Sci.* **37**, 19–46 (2009).
45. Tielke, J. A., Zimmerman, M. E. & Kohlstedt, D. L. Hydrolytic weakening in olivine single crystals. *J. Geophys. Res.* **122**, 3465–3479 (2017).
46. Richard, G., Monnereau, M. & Rabinowicz, M. Slab dehydration and fluid migration at the base of the upper mantle: implications for deep earthquake mechanisms. *Geophys. J. Int.* **168**, 1291–1304 (2017).
47. Kagi, H., Parise, J. B., Cho, H., Rossman, G. R. & Loveday, J. S. Hydrogen bonding interactions in phase A $[Mg_7Si_2O_8(OH)_6]$ at ambient and high pressure. *Phys. Chem. Miner.* **27**, 225–233 (2000).
48. Purevjav, N., Okuchi, T., Tomioka, N., Wang, X. & Hoffmann, C. Quantitative analysis of hydrogen sites and occupancy in deep mantle hydrous wadsleyite using single crystal neutron diffraction. *Sci. Rep.* **6**, 34988 (2016).
49. Purevjav, N., Okuchi, T. & Hoffmann, C. Strong hydrogen bonding in a dense hydrous magnesium silicate discovered by neutron Laue diffraction. *IUCrJ* **7**, 370–374 (2020).
50. Pacalo, R. E. & Parise, J. B. Crystal structure of superhydrous B, a hydrous magnesium silicate synthesized at 1400 °C and 20 GPa. *Am. Mineral.* **77**, 681–684 (1992).

Methods

Preparation of starting materials. Two single crystals of Mg_2SiO_4 forsterite with a size of 200–400 µm were used for the water-partition experiments between olivine and hydrous phase A: synthetic forsterite (Oxide Corporation) containing less than 1 ppm water and that containing 29 ppm water synthesized at 8 GPa and 1,800 °C for 5 h using the synthetic forsterite powder. Two kinds of experiments using these two crystals were conducted to check both normal and reverse reactions on water partitioning between forsterite and hydrous phase A. In the runs (S7420 and H5150), we used oriented synthetic forsterite crystals with dimensions of 200 µm (*a* axis) × 400 µm (*b* axis) × 400 µm (*c* axis) (Fig. 1). We also prepared hydrous silicate powdered mixtures of Mg_2SiO_4 forsterite and $Mg(OH)_2$ brucite with 8/2 mole ratio including water content of ~2.9 wt% (8Fo + 2Br) and of forsterite and brucite + SiO_2 quartz in a Mg/Si ratio of 2 with 8/2 mole ratio including water content of ~4.9 wt% (8Fo + 2[2Br + Qz]) to examine the dependence of water contents in forsterite and wadsleyite on hydration mechanisms in Mg-excess and Si-excess conditions[51,52] (Extended Data Fig. 1). Two forsterite single crystals were surrounded by these mixtures in gold capsules. The gold capsules were welded shut to avoid water escaping during experiments.

Wadsleyite single crystals used for the partition experiments were synthesized at 18 GPa and 1,800 °C for 3 h using the synthetic forsterite powder. Two pieces of wadsleyite single crystals with the grain size of ~200 µm were surrounded by the powdered mixture of 8Fo + 2Br and 8Fo + 2[2Br + Qz] in gold capsules, respectively (Extended Data Fig. 1). The experimental conditions and results are given in Extended Data Tables 1 and 2.

High-pressure and high-temperature experiments. We used 1,000 ton and 1,200 ton Kawai-type multi-anvil presses at the Bayerisches Geoinstitut, University of Bayreuth. Single crystals of forsterite and wadsleyite were synthesized with 18 mm and 10 mm Cr-doped MgO pressure media in combination with tungsten carbide (WC) anvils with 11 mm and 4 mm truncated edge lengths, respectively. The pressure media with 10 mm and 18 mm edges were used for the water-partitioning experiments using WC anvils with 5 mm and 11 mm truncated edge lengths, respectively (Extended Data Fig. 1). A $LaCrO_3$ cylindrical heater with a ZrO_2 thermal insulator was used in all experiments. Mo electrodes were located at both ends of the heater. The sample was electrically insulated from the heater using a MgO capsule. Single crystals of forsterite and wadsleyite synthesized at high pressure and high temperature were made from the synthetic forsterite power in a Re foil capsule. In experiments for the water partitioning into forsterite, the samples were heated at 8 GPa and 700 °C and at 10 GPa and 800 °C for 12–72 h, in which time dependence on water content in forsterite was examined because hydrogen diffusion in forsterite might not be sufficient to achieve hydrogen equilibrium throughout the crystal (for example, 20–75 µm at 800 °C for 5–72 h and 20 µm at 700 °C for 12 h)[53–55]. In the same manner, the samples of wadsleyite single crystals surrounded by the hydrous silicate mixtures were heated at 12 GPa and 800–900 °C for 13–14 h. The sample temperature was measured at the surface of the gold capsule using a W97%Re3%–W75%Re25% thermocouple. We made no pressure correction to the electromotive force of the thermocouple. The ceramic parts of the cell assemblies were fired at 1,273 K just before assembling them. The samples were first compressed to a desired press load at room temperature and then heated to a target temperature at a rate of ~100 °C min^{-1}. After maintaining the target temperature for the desired duration, the samples were rapidly quenched by shutting off the electric power supply of the heater and were recovered by slowly releasing the pressure. The cooling rate during quenching was estimated to be about 100 °C s^{-1}.

Analysis of the run products. The recovered sample capsules were polished, and the phases in the run products were identified using a DILOR XY Raman spectrometer and a micro-focused X-ray diffractometer equipped with a micro-focus source (IµS) of Co-Kα (Bruker, D8 Discover) with a two-dimensional solid-state detector (VÅNTEC-500). Crystal orientations of some recovered crystals after double polishing were identified using a Zeiss LEO 1530 Gemini field emission scanning electron microscope coupled with the HKL Nordlys electron back-scattered diffraction detector. Crystallographic orientation maps of the samples were analysed using Oxford Instruments HKL CHANNEL5 software.

We measured the water contents in the starting materials and recovered samples of forsterite and wadsleyite single crystals using FTIR spectroscopy with a Bruker IFS 120 high-resolution spectrometer coupled with a Bruker IR microscope. The recovered single crystals were double polished to ~50–100 µm thickness for the FTIR measurement. The water contents close to the hydrous silicate matrix with the distance of 20–50 µm were measured using FTIR. Water contents in forsterite and wadsleyite were calculated by integrating peaks using calibrations in refs. [54,55], respectively (Extended Data Table 2).

Data availability

All data used in this paper are available on Zenodo (https://doi.org/10.5281/zenodo.3936232). Any other data can be requested by emailing the corresponding author.

References

51. Beran, A. & Putnis, A. A model of the OH positions in olivine, derived from infrared-spectroscopic investigations. *Phys. Chem. Miner.* **9**, 57–60 (1983).
52. Brodholt, J. P. & Refson, K. An ab initio study of hydrogen in forsterite and a possible mechanism for hydrolytic weakening. *J. Geophys. Res. Solid Earth* **105**, 18977–18982 (2000).
53. Ingrin, J. & Blanchard, M. Diffusion of hydrogen in minerals. *Rev. Mineral. Geochem.* **62**, 291–320 (2006).
54. Withers, A. C., Bureau, H., Raepsaet, C. & Hirschmann, M. M. Calibration of infrared spectroscopy by elastic recoil detection analysis of H in synthetic olivine. *Chem. Geol.* **334**, 92–98 (2012).
55. Bolfan-Casanova, N. et al. Examination of water quantification and incorporation in transition zone minerals: wadsleyite, ringwoodite and phase D using ERDA (elastic recoil detection analysis). *Front. Earth Sci.* **6**, 75 (2018).

Acknowledgements

We thank H. Fischer for preparation of cell assemblies, R. Njul for preparation of thin-section samples, D. Wiesner and F. Ferreira for measurements of EBSD patterns of the samples and H. Keppler for measurements of water in the samples by using FTIR, at the Bayerisches Geoinstitut. We also appreciate D. J. Frost and T. Katsura for valuable discussion on this topic and T. Withers for useful comments on the manuscript. This research was supported by the Grants-in-Aid of the German Research Foundation (no. IS350/1-1) to T.I. and the Kakenhi Grants JP15H05748 and JP20H00187 from Japan Society for the Promotion of Science to E.O. E.O. was supported also by the research award from the Alexander von Humboldt foundation.

Author contributions

Both authors identified the research topic, designed the experiments, conducted high-pressure experiments and analysed the run products. Both authors discussed the results and wrote the manuscript.

Competing interests

The authors declare no competing interests.

Additional information

Extended data is available for this paper at https://doi.org/10.1038/s41561-021-00756-7.

Supplementary information The online version contains supplementary material available at https://doi.org/10.1038/s41561-021-00756-7.

Correspondence and requests for materials should be addressed to T.I.

Peer review information *Nature Geoscience* thanks Jean-Philippe Perrillat and the other, anonymous, reviewer(s) for their contribution to the peer review of this work. Primary Handling Editor: Rebecca Neely.

Reprints and permissions information is available at www.nature.com/reprints.

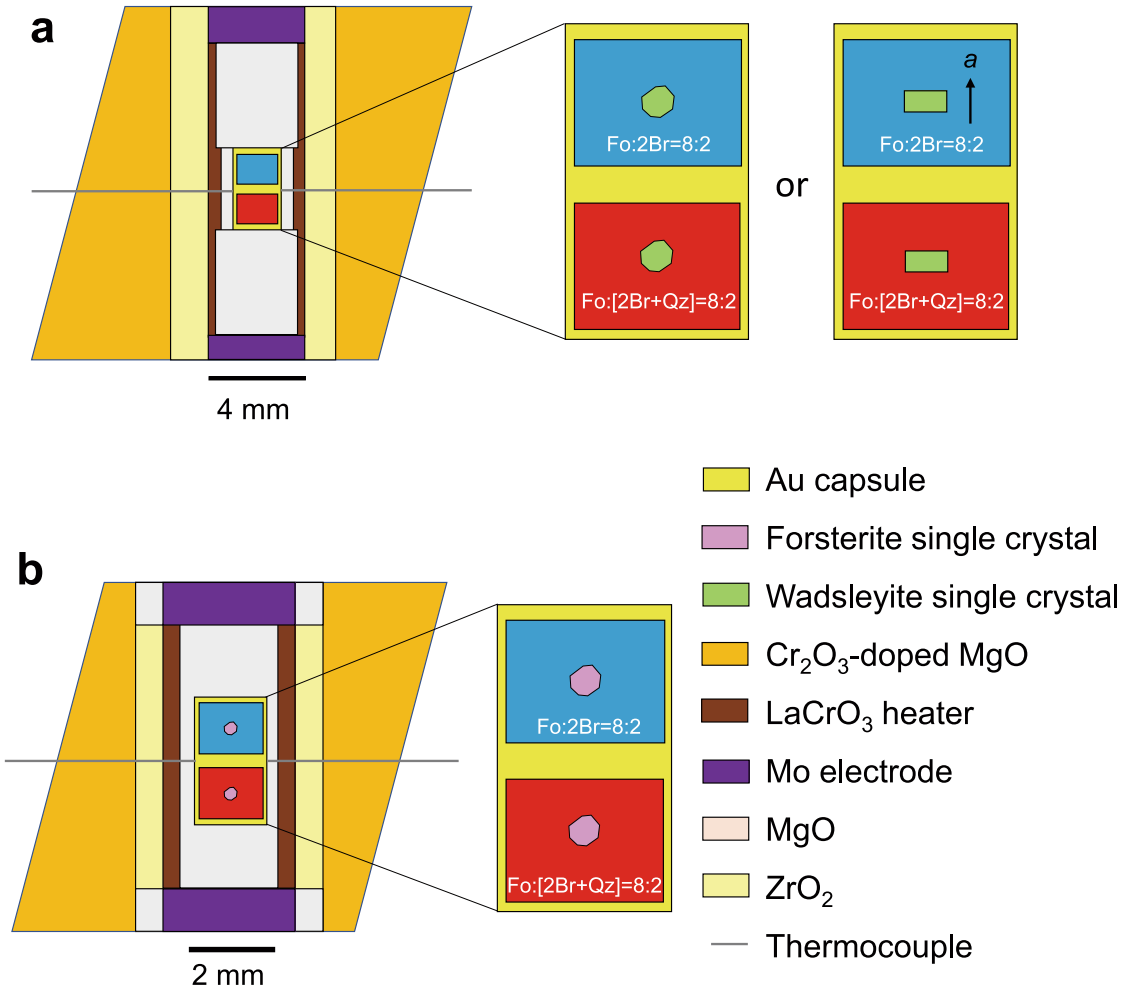

Extended Data Fig. 1 | Schematic drawings of cell assemblies. Water-partitioning experiments between **a**, forsterite and hydrous phase A and **b**, wadsleyite and hydrous phase A. In the experiments for forsterite, oriented crystals with 200 μm *a* axis × 400 μm *b* axis × 400 μm *c* axis were put in the capsules as shown in the right capsule in Extended Data Fig. 1a.

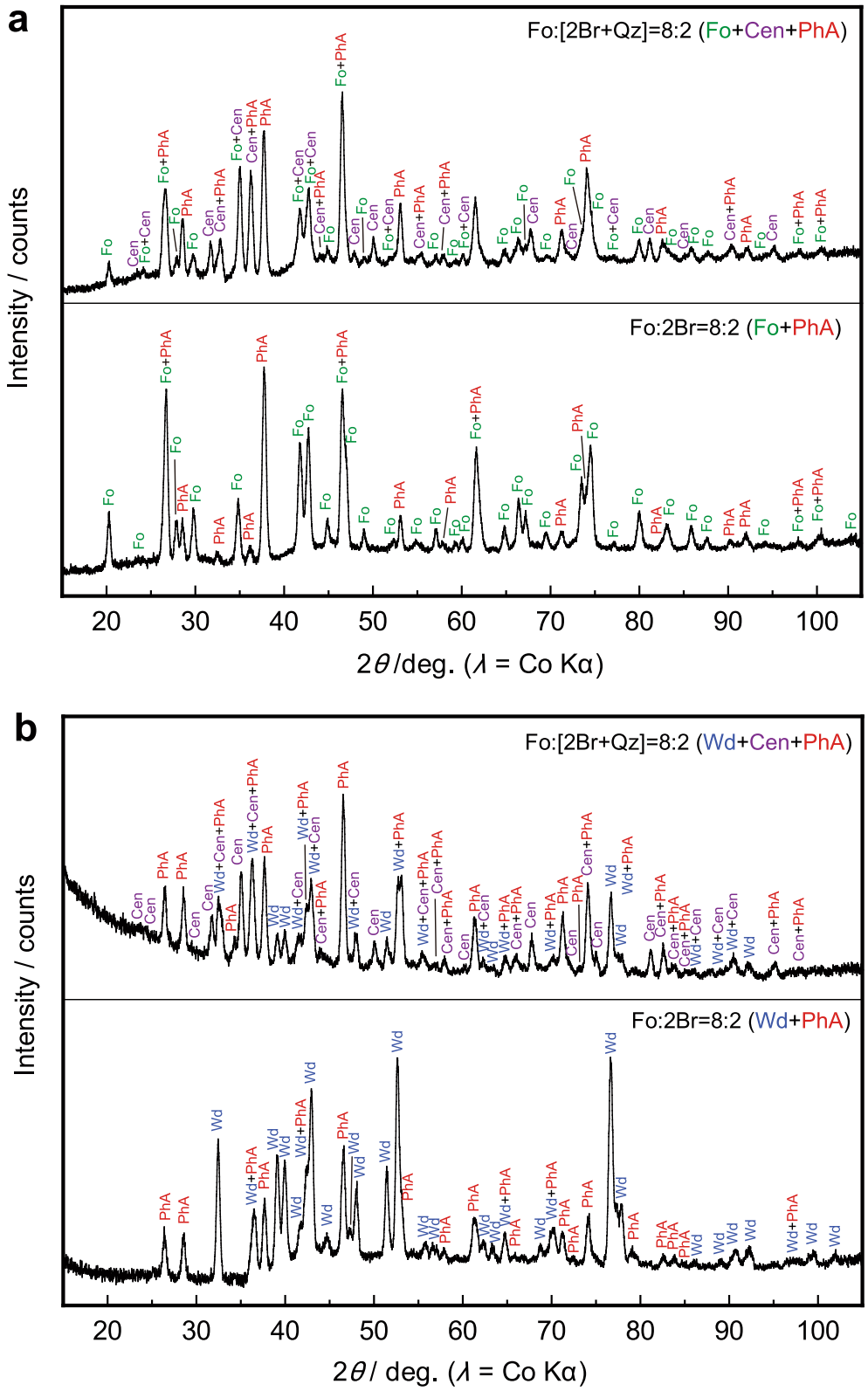

Extended Data Fig. 2 | Representative X-ray diffraction patterns of the recovered samples at the surrounding part of the single crystals. **a**, 10 GPa and 800 °C (S7423). **b**, 12 GPa and 900 °C (H5073). Fo, forsterite; Wd, wadsleyite; Cen, clinoenstatite; PhA, hydrous phase A.

R.N.	[a]S.M.	P GPa	T [o]C	Time hour	[b]Phases	H_2O content ppm wt
	Fo	-	-	-	Fo	[d]<1
H5130	Fo	8	1800	5	sFo	29(9)
H4197	Wd	18	1800	3	Wd	342(103)
H5084	Fo/8Fo+2Br	8	700	15	Fo/Fo+PhA	[c]<1
	Fo/8Fo+2[2Br+Qz]				Fo/Fo+PhA+Cen	[c]<1
S7367	Fo/8Fo+2Br	10	800	12	Fo/Fo+PhA	[c]<1
	Fo/8Fo+2[2Br+Qz]				Fo/Fo+PhA+Cen	[c]<1
S7420	Fo/8Fo+2[2Br+Qz]	10	800	72	Fo/Fo+PhA+Cen	[c]<1
S7423	sFo/8Fo+2Br	10	800	72	Fo/Fo+PhA	[c]<1
	sFo/8Fo+2[2Br+Qz]				Fo/Fo+PhA+Cen	[c]<1
H5150	Fo/8Fo+2Br	10	800	72	Fo/Fo+PhA	[c]<1
	Fo/8Fo+2[2Br+Qz]				Fo/Fo+PhA+Cen	[c]<1
H5085	Wd/8Fo+2Br	12	800	13	Wd/Wd+PhA	[d]233(70), [d]318(95)
	Wd/8Fo+2[2Br+Qz]				Wd/Wd+PhA+Cen	[d]228(68), [d]370(111)
H5073	Wd/8Fo+2Br	12	900	14	Wd/Wd+PhA	[d]273(82), [d]187(56)
	Wd/8Fo+2[2Br+Qz]				Wd/Wd+PhA+Cen	[d]249(75), [d]266(80)

Extended Data Table 1 | Experimental summary. Experimental conditions and results of phase identification and water contents in single crystals.

R.N.	[a]Phases	[b]N.M.	[c]T μm	Band frequency cm^{-1}	[e]Area cm^{-1}	[f]C_{H2O} ppm wt	[g]C.O.
	Fo	2	102	[d]none	[e]0	[e]<1	100
H5130	sFo	2	145	3491, 3568, 3579, 3612	1.18	29	649
H4197	Wd	2	100	3206, 3323, 3352	15.22	342	270
H5084	Fo/Fo+PhA	3	105	[d]none	[e]0	[e]<1	$4\bar{1}1$
	Fo/Fo+PhA+Cen	3	105	[d]none	[e]0	[e]<1	$12\bar{1}9$
S7367	Fo/Fo+PhA	3	104	[d]none	[e]0	[e]<1	$60\bar{1}$
	Fo/Fo+PhA+Cen	3	102	[d]none	[e]0	[e]<1	$10\bar{2}7$
S7420	Fo/Fo+PhA+Cen	3	134	[d]none	[e]0	[e]<1	100
S7423	sFo/Fo+PhA	3	55	[d]none	[e]0	[e]<1	$12\bar{3}\bar{2}$
	sFo/Fo+PhA+Cen	3	42	[d]none	[e]0	[e]<1	$12\bar{1}1$
H5150	Fo/Fo+PhA	3	112	[d]none	[e]0	[e]<1	100
	Fo/Fo+PhA+Cen	3	93	[d]none	[e]0	[e]<1	100
H5085	Wd/Wd+PhA	2	100	3206, 3323, 3352	[h]10.35	[h]233	$6\bar{1}\bar{2}$
				3206, 3323, 3352	[h]14.13	[h]318	$6\bar{1}\bar{2}$
	Wd/Wd+PhA+Cen	2	100	3206, 3323, 3352	[h]10.13	[h]228	1098
				3206, 3323, 3352	[h]16.43	[h]370	1098
H5073	Wd/Wd+PhA	2	100	3206, 3323, 3352	[h]12.12	[h]273	$10\bar{3}1$
				3206, 3323, 3352	[h]8.29	[h]187	$10\bar{3}1$
	Wd/Wd+PhA+Cen	2	100	3206, 3323, 3352	[h]11.05	[h]249	3511
				3206, 3323, 3352	[h]11.81	[h]266	3511

Extended Data Table 2 | Water contents of forsterite and wadsleyite. Details of FTIR measurements of forsterite and wadsleyite single crystals.